

# Flexible and Wearable All-Solid-State Supercapacitors with Ultrahigh Energy Density Based on a Carbon Fiber Fabric Electrode

Tianfeng Qin, Shanglong Peng,\* Jiaxin Hao, Yuxiang Wen, Zilei Wang, Xuefeng Wang, Deyan He, Jiachi Zhang, Juan Hou, and Guozhong Cao\*

Wearable textile energy storage systems are rapidly growing, but obtaining carbon fiber fabric electrodes with both high capacitances to provide a high energy density and mechanical strength to allow the material to be weaved or knitted into desired devices remains challenging. In this work, N/O-enriched carbon cloth with a large surface area and the desired pore volume is fabricated. An electrochemical oxidation method is used to modify the surface chemistry through incorporation of electrochemical active functional groups to the carbon surface and to further increase the specific surface area and the pore volume of the carbon cloth. The resulting carbon cloth electrode presents excellent electrochemical properties, including ultrahigh areal capacitance with good rate ability and cycling stability. Furthermore, the fabricated symmetric supercapacitors with a 2 V stable voltage window deliver ultrahigh energy densities (6.8 mW h cm<sup>-3</sup> for fiber-shaped samples and 9.4 mW h cm<sup>-3</sup> for fabric samples) and exhibit excellent flexibility. The fabric supercapacitors are further tested in a belt-shaped device as a watchband to power an electronic watch for ≈9 h, in a heart-shaped logo to supply power for ≈1 h and in a safety light that functions for ≈1 h, indicating various promising applications of these supercapacitors.


## 1. Introduction

The development of wearable electronics is gaining increasing attention due to their widespread future applications in the near future, such as in medical monitoring devices or implants,

Dr. T. Qin, Prof. S. Peng, Dr. J. Hao, Dr. Y. Wen,  
Dr. Z. Wang, Dr. D. He, Dr. J. Zhang  
Key Laboratory for Magnetism and Magnetic Materials  
of the Ministry of Education  
School of Physical Science and Technology  
Lanzhou University  
Lanzhou 730000, P. R. China  
E-mail: pengshl@lzu.edu.cn

Dr. X. Wang  
Shanghai Lishuo Composite Material Technology Co. Ltd.  
Shanghai 200335, P. R. China

Prof. J. Hou, Prof. G. Cao  
Department of Materials Science and Engineering  
University of Washington  
Seattle, WA 98195-2120, USA  
E-mail: gzcao@u.washington.edu

 The ORCID identification number(s) for the author(s) of this article can be found under <https://doi.org/10.1002/aenm.201700409>.

DOI: 10.1002/aenm.201700409

portable civilian and military equipment, and smart textiles with built-in electronic functions.<sup>[1,2]</sup> Consequently, the ever-increasing demand to power these electronics has triggered a boom in the development of flexible, lightweight and wearable energy storage units, especially in recent years. Among these numerous energy storage devices, such as supercapacitors (SCs) and lithium-ion batteries,<sup>[3–5]</sup> SCs offer high power density, excellent charge/discharge rate capability, light weight, and long life span.<sup>[6–9]</sup> However, the desired flexibility and high capacitance are not easily attainable in conventional SCs, which are unsuitable for the integration with wearable electronics.<sup>[10]</sup>

Flexible electrodes with high capacitance are key factors for achieving flexible and wearable supercapacitors with high energy density. Flexible fiber electrodes, as a promising candidate among various electrodes, have been widely studied due to their small volume and high flexibility, as well as their ease of integration into extremely small devices with tiny sizes and a variety of shapes.<sup>[6,11–16]</sup> Flexible fiber electrodes with high capacitance are commonly obtained by combining fibrous carbon or other materials as a structural support (plastic fiber, metal wire, etc.). They are highly flexible, mechanically strong and contain active materials (activated carbon particles, CNTs, graphene sheets, metal oxides, etc.).<sup>[17–21]</sup> However, there is the risk of active materials detaching from the fibrous supports due to the poor adhesion between them, especially during bending cycles. To address these challenges, flexible and high-capacity porous carbon or carbon fibers functionalized by N/O functional groups with large surface areas and desired pore volumes (including pore types) have been fabricated via various methods, such as the combination of activation and templating, activation and electrospinning, and templating and electrospinning.<sup>[22–26]</sup> Excellent electrochemical performances have been obtained because (1) Large surface area could increase the electrode/electrolyte interface that accumulates charge through electrostatic interactions;<sup>[27]</sup> (2) the unique porous structure includes micropores that are the most suitable for charge storage in the electric double layer, mesopores that provide

high-speed pathways for ion transfer to the inner surface, and macropores that act as ion-buffering reservoirs to shorten the diffusion distance of ions to the inner surface;<sup>[24,28,29]</sup> and (3) N- and O-rich functional groups, such as pyridinic N, pyrrolic N, phenolic hydroxyl and carboxyl, can generate high reversible pseudocapacitance, and quaternary N can improve electrode conductivity.<sup>[29–31]</sup> However, these electroactive carbon materials usually exist in the form of powders or short fibers, which cannot be used to fabricate flexible fiber electrodes with high mechanical strength or weaved into fabric, posing a challenge in device development.

More recently, N/O-enriched, micron-sized carbon fibers with high surface area and large pore volume (including micro/meso/macroporous) have been fabricated using the wet-spun method and exhibited excellent electrochemical performances and better mechanical strength than those made of carbon powders or short fibers.<sup>[32,33]</sup> However, the mechanical strength of these micron-sized fibers is not sufficient for weaving or knitted using a textile machine due to the large pore volume. Commercial carbon cloth with suitable strength has been used as a flexible electrode for supercapacitor. For example, an all-solid-state symmetric supercapacitor, which exhibited low capacitance and energy density, was assembled using activated carbon cloth by Li and co-workers.<sup>[34]</sup> Tong and co-workers prepared an all-solid-state asymmetric supercapacitor composed of treated commercial carbon cloth (CC) and MnO<sub>2</sub>@TiN@CC that delivered moderate capacitance and energy density.<sup>[9]</sup> However, these previous works were characterized by the following disadvantages: (1) risk of the active materials detaching from the CC in the MnO<sub>2</sub>@TiN@CC electrode mentioned above, (2) poor properties such as low capacitance and low energy density due to the small surface area (<90 m<sup>2</sup> g<sup>-1</sup>) (3) difficult to integrate to smart/wearable electronics. Thus, preparing flexible carbon fibers with high capacitance for weaving and further fabricating flexible and wearable supercapacitors is an urgent issue to be resolved.

In this work, N/O-enriched carbon microfibers cloth (CC) with large surface area and desired pore volume were obtained through combined wet-spinning and KOH activation and textile technology. The subsequent electrochemical treatment resulted in an increased specific surface area and pore volume of the carbon cloth, and the introduction of electrochemical functional groups to the carbon surface. The treated CC electrode material delivered high areal capacitances of 2.36 F cm<sup>-2</sup> as the positive electrode and 1.70 F cm<sup>-2</sup> as the negative electrode in 1 M Na<sub>2</sub>SO<sub>4</sub>, excellent rate ability, and super cycling stability. The fabricated symmetric devices with a 2 V stable voltage window demonstrated ultrahigh energy densities (13.6 mW h cm<sup>-3</sup> for a single bundle of carbon fibers, 6.8 mW h cm<sup>-3</sup> for the fiber-shaped device, and 9.4 mW h cm<sup>-3</sup> for the fabric device). In addition, superior flexibility of the fabricated device (maintaining 85% of its initial capacitance after 200 cycles of bending at 720°) was achieved. More importantly, a device with a size of 2 × 10 cm<sup>2</sup>-sized powered an electronic watch as the watchband, a heart-shaped logo composed of 10 red light-emitting diodes (LEDs) in parallel, and a safety light composed of 10 green LEDs in parallel for ≈9, 1, and 1 h, respectively, representing further promising applications of the devices in wearable electronics now or in the future.

## 2. Results and Discussion

CC, CC electrochemically treated for 3 min (3-CC), pristine carbon microfiber bundles (CMF) and electrochemically treated carbon fiber bundles (3-CMF) with electrochemical treatment all demonstrated excellent mechanical strength and flexibility during deformation testing, and it was found that CC and 3-CC do not crack when they are wound on a glass rod with a diameter of ≈6 mm or even folded into bow ties; after the unfolding, CC and 3-CC still remain pristine in appearance (≈2 × 13.5 cm<sup>2</sup>) (Figure 1a–c). Pristine carbon fiber bundles and electrochemically treated carbon fiber bundles with electrochemical treatment can be folded into three circles of a logo (Figure 1d,e) and weaved into ≈1 × 5 cm<sup>2</sup> areas of cloth with cotton threads (Figure 1f), the weaving process is shown in Schematic S1 in the Supporting Information, which indicates the favorable mechanical strength of the electrodes, which only minimally changes upon deformation and meets the requirement for wearable supercapacitor electrodes, even after electrochemical oxidation. Scanning electron microscopy (SEM) was employed to further detect the morphological variations in CC, 3-CC, CMF, and 3-CMF and their changes after electrochemical oxidation. Crossed warp and weft composed of a CMF bundle with a diameter of ≈400 μm can be clearly observed (Figure 1g), wherein the CMF has a diameter of ≈7 μm (upper right corner of the inset). After oxidation, the surface grooves and embossments become deeper and clearer compared to the pristine sample (Figure 1h,i). High-magnification SEM images at different oxidation times (1, 7, and 11 min) were also performed to clarify the effect of oxidation time on surface morphology (Figure S1a–c, Supporting Information): longer electrochemical oxidation times lead to deeper grooves and clearer embossments due to the ongoing redox reactions between carbon and the mixed acid.

High-magnification transmission electron microscopy (TEM) images indicate that CC is composed of ≈100 nm nanorods coated with ≈50 nm nanoparticles (Figure 2a). After electrochemical oxidation, the diameters of the nanoparticles decrease and become unclear (Figure 2b). The surface area and pore width distribution were analyzed by nitrogen adsorption isotherms at 77 K. CC and 3-CC adsorption isotherms all show typical type I behavior according to the IUPAC classification. The rapid increase in the adsorption isotherms at low  $P/P_0$  (close to zero) indicates the presence of micropores (Figure 2c). Two sharp peaks are centered at ≈1.94 and ≈1.93 nm for CC and 3-CC, respectively (the inset of Figure 2c). However, the pore-size distributions are similar. Pores less than 2 nm are generally not reliable for the Barrett–Joyner–Halenda (BJH) analysis, because the capillary condensation of N<sub>2</sub> is not sure in the region.<sup>[35]</sup> Thus, the same pore-size distribution tested by BJH analysis may not indicate the true situation of the pore-size distributions of our pristine and treated sample. An excellent high surface area of 419.85 m<sup>2</sup> g<sup>-1</sup> and an approximate pore volume of 0.23 cm<sup>3</sup> g<sup>-1</sup> are obtained for CC. After electrochemical oxidation treatment, the surface area and pore volume reach up to 468.59 m<sup>2</sup> g<sup>-1</sup> and 0.25 cm<sup>3</sup> g<sup>-1</sup>, respectively, indicating the importance of the simple and fast electrochemical oxidation in increasing the surface area and pore volume. Raman spectra of CC and 3-CC show typical D (1354 cm<sup>-1</sup>) and G (1597 cm<sup>-1</sup>)

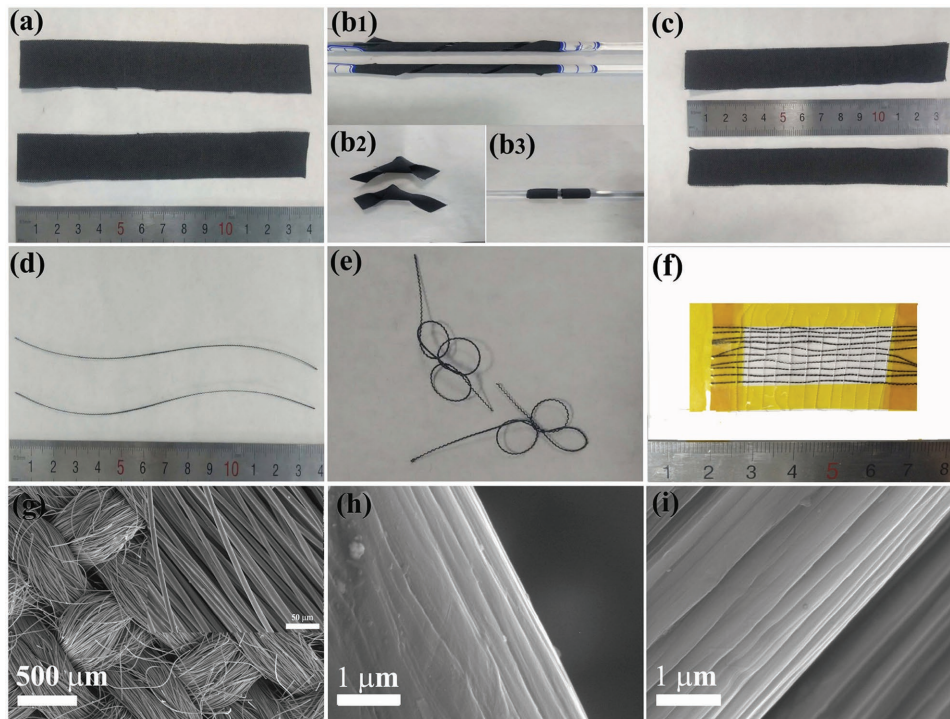


**Figure 1.** Morphological characterization of carbon fibers, CC and 3-CC. a) Optical images of CC (up) and 3-CC (down) before shape changing, b<sub>1</sub>, b<sub>2</sub>) wound on glass rod, b<sub>2</sub>) kinked, c) after shape changing, d) bundles of pristine carbon fiber (up) and carbon fiber with electrochemical treatment (down), e) kinked, f) weaved with white cotton threads. g) SEM images of CC (the inset: its high magnification image) and h) of pristine carbon fiber at high magnification and i) with electrochemical treatment.

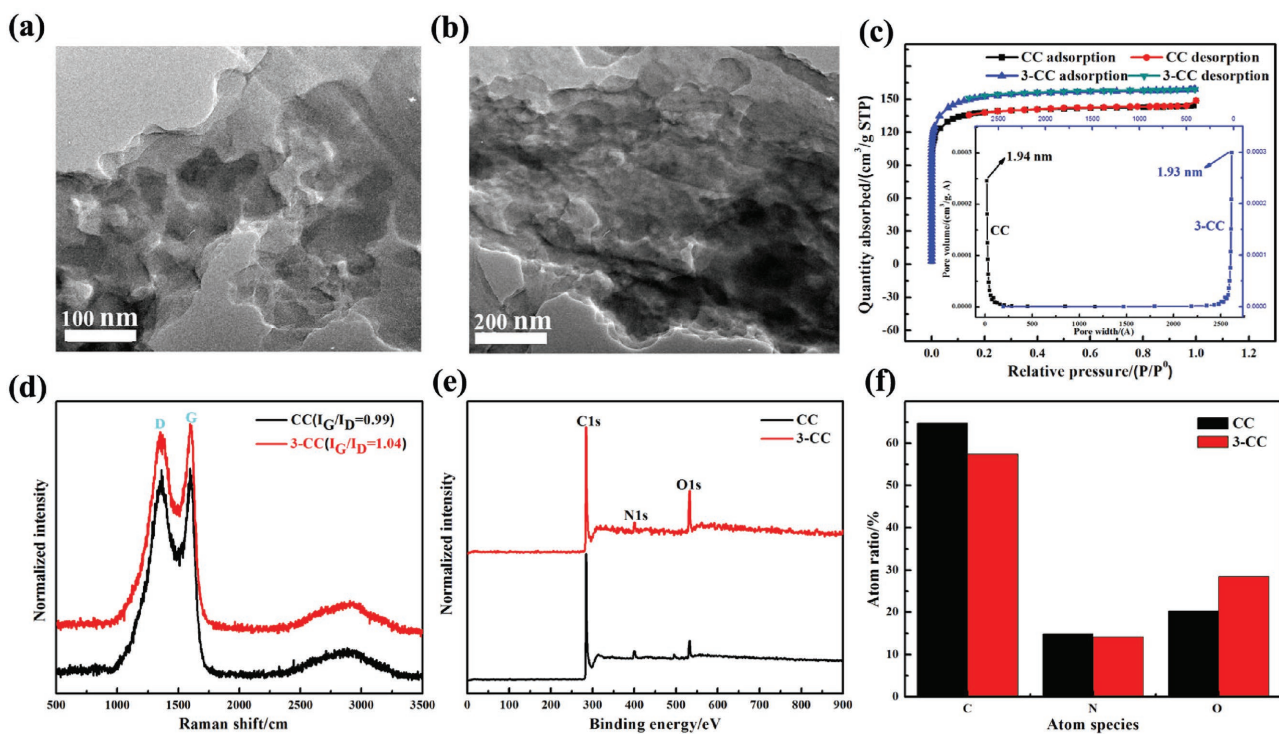
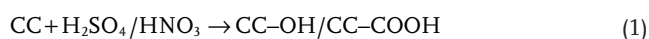


**Figure 2.** a, b) High-magnification TEM images, c) BET surface area (the inset: BJH pore width distribution), d) Raman spectra, e) XPS full spectra, and f) relative atom ratio of CC and 3-CC.

peaks (Figure 2d), where the G band represents the in-plane bond-stretching motion of pairs of C  $sp^2$  atoms ( $E_{2g}$  phonons), while the D band corresponds to breathing modes of rings or K-point phonons of  $A_{1g}$  symmetry.<sup>[36–38]</sup> After oxidation treatment, the intensity ratio  $I_G/I_D$  increases from 0.99 for CC to 1.04 for 3-CC, indicating an increase in the average size of the  $sp^2$  domain on the surface of 3-CC and a decrease in the degree of disorder.<sup>[39]</sup> X-ray photoelectron spectroscopy (XPS) analysis was conducted to obtain the surface elements and bonding states of the samples. Three sharp peaks centered at  $\approx 284$  eV (C1s),  $\approx 400$  eV (N1s), and  $\approx 532$  eV (O1s) appear in the XPS spectrum of CC (Figure 2e). After oxidation treatment, the atomic ratio of C and N decreases and that of O increases, as obtained by integration of the full spectra (Figure 2f). The introduction of O functional groups into the surface of the carbon fiber or CC corresponds to the following equation<sup>[40]</sup>



where  $sp^3$ -hybridized carbon loses electrons and bonds with  $O^{2-}$  to form  $-C-OH$  and  $-COOH$ , and  $S^{6+}$  and  $N^{5+}$  obtain electrons to produce  $SO_2$  and  $NO_2$ . The  $60^\circ C$  is replaced by a constant voltage of 3 V in our method, and the 3 V of voltage employed in our experiment decreases the reaction barrier and increases the rate of reaction (1), producing a similar effect as the  $60^\circ C$ . The increasing content of C–O and the emergence of C–OH confirmed by XPS analysis in Figures S2 and S8c in the Supporting Information are also corresponding to the Equation (1). The full spectra and atomic ratio of the samples that underwent different oxidation times (1, 7, and 11 min) were also recorded to clarify the effect of oxidation time on the ratio of different elements (Figure S2, Supporting Information).

The atomic ratio of C and N gradually decreases and that of O increases with prolonged oxidation time, indicating the importance of simple electrochemical oxidation on adjusting the elements and different functional group ratios.

The energy density of the supercapacitor was calculated according to the equation  $E = CV^2/2$ , where  $C$  is the capacitance, and  $V$  is the voltage of the device.<sup>[41]</sup> Thus, a high capacitance of the electrode and a wide potential of the device are essential for achieving a high energy density. The optimized time of 3 min, derived from the electrochemical process, was first confirmed by detecting the capacitive performance of the electrodes at different treatment times (Figure S3, Supporting Information). The optimized 3-CC electrode delivered a high capacitance of  $2.4 \text{ F cm}^{-2}$  at a current density of  $1 \text{ mA cm}^{-2}$  as the positive electrode in  $1 \text{ M Na}_2\text{SO}_4$  of electrolyte. Using CC or 3-CC for both the negative and positive electrode, the CV curves of CC and 3-CC present a rectangular shape, indicating good capacitive behavior (Figure 3a). The charge/discharge times of 3-CC as the positive and negative electrode are  $\approx 4227$  and  $\approx 4098$  s, which are larger than those of CC of  $\approx 2600$  and  $\approx 2800$  s, indicating the excellent charge storage capability of 3-CC (Figure 3b). It is exciting that ultrahigh areal capacitances of  $\approx 2.4$  and  $\approx 1.7 \text{ F cm}^{-2}$  are obtained for 3-CC as the positive and negative electrode, which are higher than the capacitances of CC of  $\approx 1.3$  and  $\approx 1.5 \text{ F cm}^{-2}$ , respectively (Figure 3c,d), and much higher than the values of recently reported carbon-based materials and some metal oxide anodes (Figure S4 and Table S1, Supporting Information). Furthermore, the volumetric capacitance can reach up to  $\approx 49 \text{ F cm}^{-3}$  (3-CC as the positive electrode),  $\approx 25 \text{ F cm}^{-3}$  (CC as the positive electrode),  $\approx 35 \text{ F cm}^{-3}$  (3-CC as the negative electrode), and  $\approx 29 \text{ F cm}^{-3}$  (CC as the negative electrode). Low resistances,

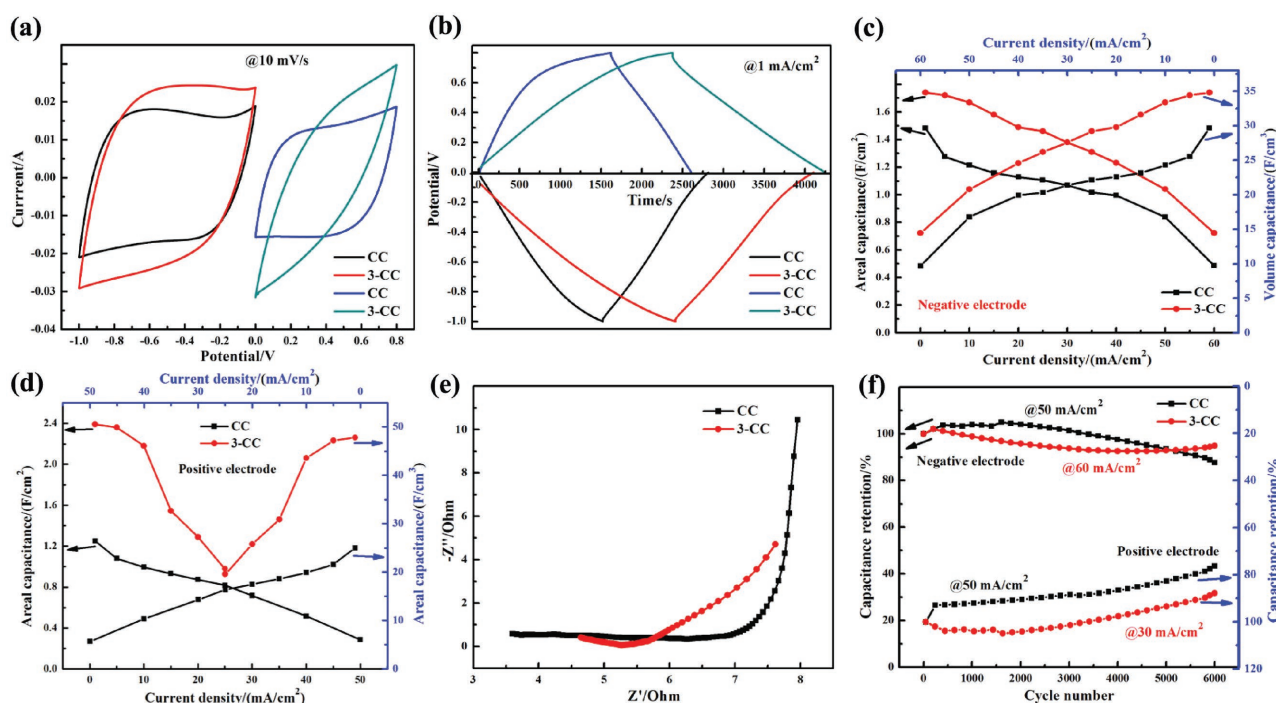
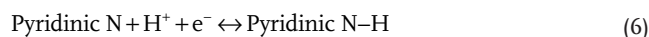
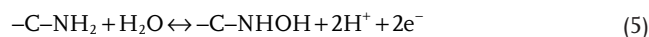


**Figure 3.** Comparison of a) CV curves, b) galvanostatic charge/discharge (GCD) curves, c,d) rate capabilities, and f) cycling performance of CC and 3-CC as negative and positive electrodes. e) Nyquist plots of CC and 3-CC.

such as equivalent series resistance ( $E_{SR}$ ) and charge transfer resistance ( $R_{CT}$ ), are observed over a narrow coordinate range of 0–9  $\Omega$  for the  $x$ -axis and 0–12  $\Omega$  for the  $y$ -axis (Figure 3e). In the high-frequency region, the intercept at the real part ( $Z'$ ) represents the combined resistance of the electrolyte ionic resistance, the substrate intrinsic resistance, and the contact resistance at the active material/current collector interface.<sup>[42]</sup> The  $E_{SR}$  value of 3-CC is 4.6  $\Omega$ , larger than that of CC of 3.55  $\Omega$  due to the increasing oxygen content. No obvious semicircles are observed for either CC or 3-CC, indicating the low  $R_{CT}$  value caused by faradaic redox reactions and the double-layer capacitance on the surface of the electroactive material.<sup>[42]</sup> Both CC and 3-CC electrodes exhibit inclination angles of  $\approx 90^\circ$ , indicating ideal capacitive behavior. These favorable parameters correspond to the excellent capacitances mentioned above. After 6000 cycles, capacity retentions of  $\approx 88\%$  for CC and  $\approx 95\%$  for 3-CC as the negative electrode and  $\approx 76\%$  for CC and  $\approx 88\%$  for 3-CC as the positive electrode are obtained, indicating excellent long-term cycling stability (Figure 3f). All these parameters, including the wide potential range of  $-1$ – $0.8$  V, high capacitances of  $\approx 2.4$  and  $\approx 1.7$  F  $\text{cm}^{-2}$  as the positive and negative electrode for 3-CC, excellent rate capability, and long-term cycling stability, contribute to the realization of the high-performance supercapacitor. In addition, CC and 3-CC also exhibit superior capacitive and rate capabilities in acidic and basic electrolytes (Figures S5 and S6, Supporting Information). Ultrahigh capacitances of  $\approx 6.29$  F  $\text{cm}^{-2}$  for 3-CC and  $\approx 3.00$  F  $\text{cm}^{-2}$  for CC as the negative electrode in 6 M KOH are obtained along with the excellent rate capability; for example, when the charge/discharge current density increases to 166.67 mA  $\text{cm}^{-2}$  (0.25 A, the upper limit of the current for the electrochemical station CHI660E), a capacitance of  $\approx 433.88$  mF  $\text{cm}^{-2}$  was maintained. In addition, excellent rate capability and capacitances of  $\approx 5.01$  F  $\text{cm}^{-2}$  for 3-CC and  $\approx 2.75$  F  $\text{cm}^{-2}$  for CC in 1 M  $\text{H}_2\text{SO}_4$  are exhibited (Figure S6, Supporting Information). High mass capacitances are obtained, including  $\approx 329.53$  for 3-CC and  $\approx 144.02$  F  $\text{g}^{-1}$  for CC as the negative electrode in 6 M KOH electrolyte and  $\approx 238.88$  for 3-CC and  $\approx 132.54$  F  $\text{g}^{-1}$  for CC as the positive electrodes in 1 M  $\text{H}_2\text{SO}_4$  electrolyte (Figure S7, Supporting Information).

To clarify the reasons behind the enhanced electrochemical properties, the effect of functional groups on the capacitive performance of the CC and 3-CC electrodes that underwent different electrochemical oxidation times was first studied by fitting the narrow XPS spectra (Figure S8, Supporting Information). With prolonged electrochemical oxidation time, the content of the elements varies (Figure S2, Supporting Information): O increases, N decreases a little, and C decreases. O and N can contribute to the capacitance through redox reactions, indicating that these elements are directly responsible for the improved capacitance, particularly O in this work.<sup>[29]</sup> The mechanisms inducing pseudocapacitance can be depicted through the following reactions<sup>[40,43]</sup>



The 3-CC electrode shows the highest capacitance at an optimized O/N/C ratio of 2.02:0.50:1 and a C=O/C–O/C–OH ratio of 2:34.88:1, as calculated from Figure S8 (Supporting Information). Obviously, C–O functional groups clearly play a more important role in enhancing the capacitance than C=O or C–OH. In addition, the high surface area such as 419.85 m<sup>2</sup> g<sup>−1</sup> for CC and 468.59 m<sup>2</sup> g<sup>−1</sup> for 3-CC, can store high amounts of charge via electrostatic interactions at the electrode/electrolyte interface; the microporous nature of CC and 3-CC highly contribute to the enhanced capacitance as described in the introduction. In brief, the excellent and enhanced electrochemical properties are due to the high surface area contributed by the high electric double layer capacitance and the N/O-rich functional groups, thus generating Faradaic pseudocapacitance.

Based on the outstanding properties of the above electrodes and the reversibility of the transformation from a fiber-shaped device to a fabric device, both fiber-shaped and fabric devices were fabricated and both indicated excellent long-term cycling, ultrahigh energy density, and superflexibility as wearable energy storage devices. In addition, the masses of the different parts of the supercapacitors are included in Figure S9 in the Supporting Information. The fiber-shaped device based on CC delivers a higher length capacitance of  $\approx 32$  mF  $\text{cm}^{-1}$  than the device based on CC of  $\approx 20$  mF  $\text{cm}^{-1}$  (Figure 4b) and much higher than the values for recently reported fiber-shaped supercapacitors (Figure S10, Supporting Information). And better rate capabilities are obtained for the fiber-shaped device based on CC compared with that based on 3-CC due to the lower oxygen content. The cyclic stabilities of the fiber-shaped devices based on CC and 3-CC were evaluated through galvanostatic charge/discharge (GCD) tests (Figure 4c), where  $\approx 99\%$  and  $\approx 90\%$  of the capacitances of the devices based on CC and 3-CC were maintained after 2100 cycles, demonstrating excellent stabilities. Ragone plots were employed to assess the energy storage capability of the devices for energy storage (Figure 4d). In addition, the diameter of the carbon fiber bundle and the thickness of CC are 400  $\mu\text{m}$  and 500  $\mu\text{m}$ , respectively, as shown in Figure S11 in the Supporting Information. The volume energy density of the device based on 3-CC was  $\approx 6.8$  mW h  $\text{cm}^{-3}$ , which is higher than that of the device based on CC of  $\approx 1.6$  mW h  $\text{cm}^{-3}$  and much higher than the recently reported values of recently reported fiber-shaped supercapacitors (Figure S12, Supporting Information). The volumetric energy density based on the single fiber bundle electrode of 3-CC was  $\approx 13.6$  mW h  $\text{cm}^{-3}$ , which is higher than that of a CC single fiber bundle of  $\approx 3.2$  mW h  $\text{cm}^{-3}$ . Mass energy density is another parameter used to evaluate the properties of a device. The energy density of the device based on 3-CC is  $\approx 6.6$  W h  $\text{kg}^{-1}$  based on the mass of two electrodes, and  $\approx 52$  mW h  $\text{kg}^{-1}$  based on the mass of the entire device with power densities of  $\approx 51.66$  W  $\text{kg}^{-1}$  and  $\approx 407$  mW  $\text{kg}^{-1}$ , which are higher than those of the CC device based on CC of  $\approx 1.5$  W h  $\text{kg}^{-1}$  and  $\approx 11.5$  mW h  $\text{kg}^{-1}$  with power densities of  $\approx 24$  W  $\text{kg}^{-1}$  and  $\approx 190$  mW  $\text{kg}^{-1}$ . In addition, the fiber-shaped devices based on both 3-CC and CC retain their good electrochemical properties under various bending states

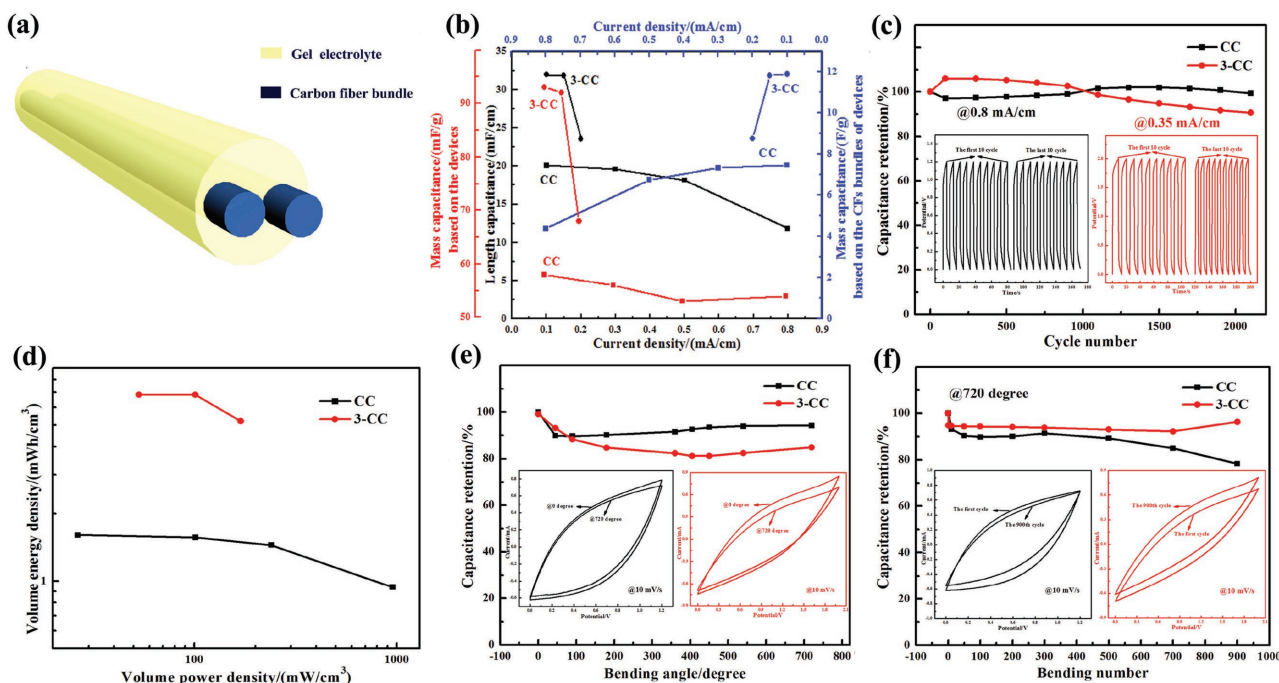


**Figure 4.** Electrochemical performances of two fiber-shaped supercapacitors based on CC and 3-CC carbon fibers bundles. a) Structure schematic for fiber-shaped SC. b) Rate capabilities based on GCD testing at different densities, c) cycling stability, and d) Ragone plots. Capacitance retention under e) bending over  $0^{\circ}$  to  $720^{\circ}$  (the inset: CV curves before and after bending), and f) bending stabilities at  $720^{\circ}$  (the inset: CV curves before and after bending cycles).

and cycles, indicating superior flexibility (bending into two circles including one circle in the positive direction and one circle in the negative directions), which is essential for wearable energy storage devices. For example,  $\approx 94\%$  and  $\approx 85\%$  capacitance is maintained while bending the devices based on CC and 3-CC, respectively, even for angles ranging from  $0^{\circ}$  to  $720^{\circ}$  (Figure 4c,e). Moreover,  $\approx 97\%$  of the capacitance of the device based on 3-CC is maintained after 900 cycles at  $720^{\circ}$ , which is higher than that of the device based on CC of  $\approx 79\%$  (Figure 4f). The fiber-shaped device exhibits more promising applications (Figures S13 and 14, Supporting Information). For instance, a supercapacitor composed of devices based on CC and 3-CC in series could light a yellow LED (2 V, 20 mA) for at least 10 min.

Symmetric devices with both a stable voltage window of 2 V and LiCl/PVA gel as the electrolyte based on both CC and 3-CC exhibit excellent properties as good as the fiber-shaped devices, such high areal capacitance, ultrahigh volume energy density, superior flexibility, and promising applications, comparable to the fiber-shaped devices (Figure 5). The charging/discharging time reaches up to  $\approx 6483$  s, indicating the excellent charge storage capability of the 3-CC-based device compared with the CC-based device ( $\approx 5176$  s, Figure 5b) and a larger IR of the 3-CC-based device compared with the CC-based device due to the increased oxygen content. After 5100 cycles,  $\approx 122\%$  and  $\approx 116\%$  retention of the initial capacitance is retained for the devices based on CC and 3-CC, thus demonstrating excellent stabilities, where the increased capacitance could be due to the electrochemical activation. Ragone plots are introduced to evaluate the capability of the devices for energy storage (Figure 5d). The fabric device based on 3-CC exhibits ultrahigh

volume energy density of  $\approx 9.4$  mW h  $\text{cm}^{-3}$  at high power density of  $\approx 13$  mW  $\text{cm}^{-3}$ , which are higher than the volume energy density of  $\approx 6.2$  mW h  $\text{cm}^{-3}$  at power density of  $\approx 10$  mW  $\text{cm}^{-3}$ , while both energy densities are much higher than the recently reported values of recently reported planar supercapacitors (Figure S15, Supporting Information). Moreover, the 3-CC based fabric device delivers a higher energy density of  $\approx 24.77$  W h  $\text{kg}^{-1}$  considering the mass of the two electrodes ( $\approx 95.1$  mg) or  $\approx 3.66$  W h  $\text{kg}^{-1}$  considering the total mass of the two electrodes, the solid electrolyte and the separator (0.3963 g) than the CC-based device, with respective energy densities of  $\approx 15.22$  W h  $\text{kg}^{-1}$  ( $\approx 105.65$  mg) and  $\approx 2.47$  W h  $\text{kg}^{-1}$ . The mass energy densities of the entire 3-CC- and CC-based devices reach  $\approx 1.69$  W h  $\text{kg}^{-1}$  and  $\approx 1.14$  W h  $\text{kg}^{-1}$ , respectively, for which the average mass of the device is  $\approx 1.37$  g (CC-based device: 1.28 g; 3-CC-based device: 1.46 g), and the active electrode/device ratio is  $\approx 6.94\%$  for the 3-CC device and  $\approx 7.7\%$  for the CC device. The mass ratio of CC, solid electrolyte and separator to the device, Ni belt device and packaging materials are  $\approx 50\%$ ,  $\approx 33\%$ , and  $\approx 17\%$ , respectively. The 3-CC and CC-based fabric devices exhibit excellent capacitance retention under various bending states and cycles, indicating superior flexibility, which is vital for wearable energy storage devices. For example,  $\approx 103\%$  and  $\approx 89\%$  capacitance retention is achieved for 3-CC- and CC-based devices, respectively, under bending, even with angles ranging from  $0^{\circ}$  to  $720^{\circ}$  (Figure 5e). Moreover,  $\approx 90\%$  capacitance retention for the device based on CC is maintained after 210 cycles at  $720^{\circ}$ , which is higher than that of the device based on 3-CC, with  $\approx 85\%$  capacitance retention (Figure 5f). The fabric supercapacitors based on both CC and 3-CC demonstrate additional

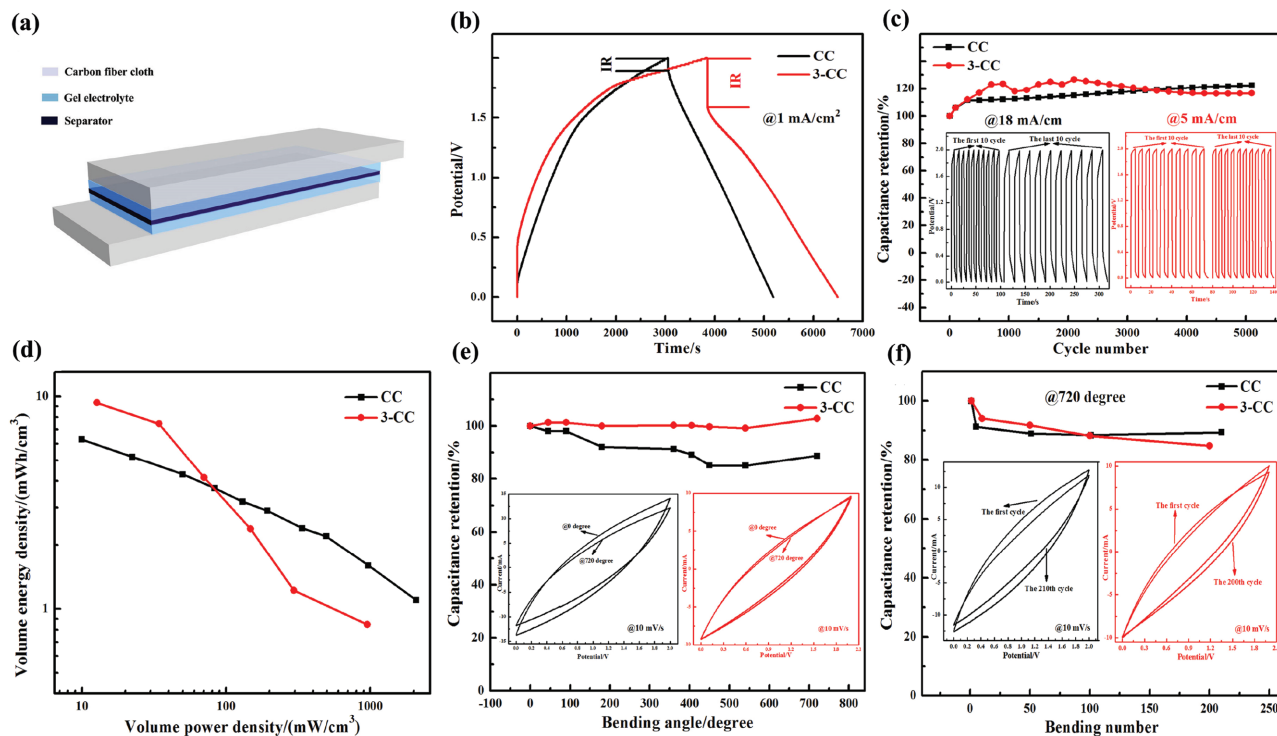


**Figure 5.** Electrochemical performance of two fabric supercapacitors based on CC and 3-CC. Structure schematic for a) planar SC, b) GCD curves, c) cycling stability, and d) Ragone plots. e) Capacitance retention under bending ranging from 0° to 720° (the inset: CV curves before and after bending), and f) bending stabilities at 720° (the inset: CV curves before and after bending).

promising applications. For instance, a single supercapacitor based on CC or 3-CC could light a red LEDs (2 V, 20 mA) for at least 60 min (Figures S16 and S17, Supporting Information).

Our large-sized supercapacitors based on 3-CC (LSSC, Figures S18 and 19, Supporting Information) exhibit promising application that are close to commercialization in various fields. For instance, inspired by a bundle of heart-shaped red roses that could be presented in a marriage proposal, a heart-shaped logo composed of 10 red LEDs in parallel was lighted and lasted for at least 60 min, which could be enough time for a proposal in a romantic atmosphere (Figure 6a<sub>1</sub>–a<sub>4</sub>). A single LSSC as a watchband and power source can power an electronic watch for ≈9 h, representing major huge commercial prospects (Figure 6b<sub>1</sub>–b<sub>4</sub>). In addition, a safety light for safe escape composed of 10 green LEDs in parallel was lighted and lasted 60 min, which could be used as emergency fire-escape lighting in buildings (Figure 6c<sub>1</sub>–c<sub>4</sub>). After three crevices were cut in the LSSC, ≈60% capacitance retention was obtained after three crevices were cut in the LSSC (Figure S20b,c, Supporting Information). The self-discharge and leakage current of 3-CC devices (small size of 2 cm<sup>2</sup> and large size of 20 cm<sup>2</sup>) also were tested and the results are shown in Figure S21 in the Supporting Information. The self-discharge processes of the two devices are similar (Figure S21a, Supporting Information). For example, after self-discharge for 14.8 h the voltage decreased to 0.89 V for small device and 0.7 V for large device, indicating ≈50% retention of the cell voltage. The leakage current of two devices are shown in Figure S21b in the Supporting Information; after ≈10 h the leakage current decreases

to 0.2 mA for the small device and 0.53 mA for the large device.

The comparison of the present study with the data reported in literature is shown in Tables S2 and S3 in the Supporting Information. It can be seen that the excellent electrochemical performance is due to the larger surface area of pristine carbon cloth in our experiment. The increased specific surface area and oxygen content for carbon cloth in our experiment through electrochemical treatment are almost as much as that of the reported literatures. But the enhanced electrochemical performance such as capacitances and energy densities are much larger than that of the reported literatures. Obviously, the large surface area of pristine CC used in our experiment makes greater contribution to the enhanced performance than that of heteroatom doping, etc. Besides, the heteroatom doping such as O and N only make a remarkable contribution to the excellent electrochemical performance while the pristine carbon cloth inherits large surface area as shown in Tables S2 and S3 in the Supporting Information. This type of carbon cloth is employed as electrode for the first time to prepare the flexible all-solid-state device after simple electrochemical treatment, demonstrating promising practical application. The enhancement of electrochemical properties of electrodes/devices is ascribed to the large specific surface area and pore volume as well as the introduction of oxygen containing functional groups to the carbon fiber (Table S2, Supporting Information). Similar results have been reported and discussed in literature. For example, Li group employed tedious chemical oxidation/reduction method to enhance the electrochemical properties of

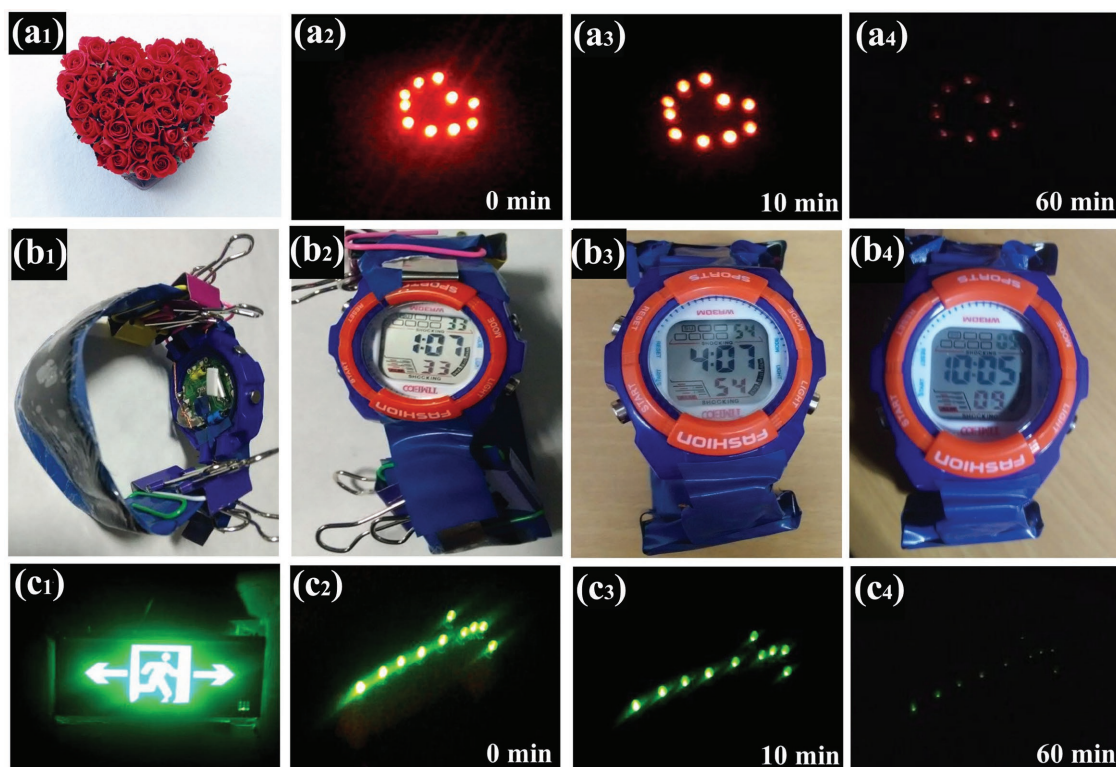


**Figure 6.** Large-sized supercapacitor (LSSC) of  $2 \times 10 \text{ cm}^2$  based on 3-CC. Heart-shaped image composed of a<sub>1</sub>) red roses and a<sub>2–a4</sub>) heart-shaped logo consisting of 10 red LEDs in parallel and lit up by a single LSSC. b<sub>1</sub>) Electronic watch with the LSSC as the watchband. b<sub>2–b4</sub>) Electronic watch powered by the LSSC watchband. c<sub>1</sub>) Image of a safety sign and c<sub>2–c4</sub>) safety indication arrow composed of 10 green LEDs in parallel and lit up by the LSSC and two small-sized devices in series, in which the two devices are in parallel.

electrode/device.<sup>[34]</sup> Tong and co-workers utilized electrochemical exfoliation in mixed acid for 10 min to obtain high-performance carbon fiber electrode.<sup>[9]</sup> Fisher and co-workers reported the electrochemical oxidation treatment in 1 M of  $\text{H}_2\text{SO}_4$  to get carbon electrode.<sup>[33]</sup>

### 3. Conclusions

N/O-enriched carbon fiber cloth with large surface area and desired pore volume has been fabricated. A simple and efficient electrochemical treatment is used to further optimize the properties of CC. With good flexibility, ultrahigh areal capacitance, and excellent rate ability, the CC and treated CC were used as electrodes to assemble flexible all-solid-state symmetric capacitors with LiCl/PVA as a gel electrolyte. Both the planar and the fiber-shaped devices exhibit ultrahigh energy densities of  $9.4 \text{ mW h cm}^{-3}$  for the fabric device,  $6.8 \text{ mW h cm}^{-3}$  for the fiber-shaped device, and  $13.6 \text{ mW h cm}^{-3}$  for the single bundle of carbon fibers. The excellent performances can be ascribed to synergistic combination of the large specific surface area and the desired pore volume with surface electrochemical active functional groups, which enhance the electric double-layer capacitance and contribute to Faradaic pseudocapacitance. A large-sized supercapacitor was tested as both a watchband and a power source to power an electronic watch for  $\approx 9 \text{ h}$ , demonstrating promising commercial applications.

### 4. Experimental Section

**Fabrication of CMF and CC:** In cooperating with Shanghai Lishuo composite materials Co. Ltd., high surface area of porous CMF with rich N/O functional groups was fabricated by combining wet-spun with KOH activation. Bundles of toughness reinforced CMF were then weaved into large-sized CC using textile technology.

**Fabrication of 3-CC:** The 3-CC was obtained by electrochemical oxidation treatment. Before oxidation treatment, large-sized CC was cut into strips ( $\approx 1 \times 1.5 \text{ cm}^2$ , mass per unit area  $\approx 21 \text{ mg cm}^{-2}$ , thickness:  $\approx 500 \mu\text{m}$ ). Electrochemical oxidation treatment was carried out in a standard three electrode cell in a mixed acid of  $\text{HNO}_3$  and  $\text{H}_2\text{SO}_4$  (V:V = 29 mL:29 mL) with a platinum sheet as counter electrode and a saturated calomel electrode (SCE) as a reference electrode under a constant voltage of 3 V. Processing times of 1, 3, 7, and 11 min were applied for each carbon CC strips. Finally, the CC strips were washed with deionized water after treatment and dried at  $60^\circ\text{C}$ . The mass per unit area of 3-CC is  $\approx 19 \text{ mg cm}^{-2}$ .

**Assembly of All-Solid-State Supercapacitors:** To prepare the gel electrolyte,  $\approx 6 \text{ g}$  of LiCl and  $\approx 3 \text{ g}$  of polyvinyl alcohol (PVA) were mixed with  $\approx 30 \text{ mL}$  of deionized water. The above mixture was then heated to  $90^\circ\text{C}$  under vigorous stirring until it became clear. After soaking separators and electrodes with gel electrolyte, the separator was sandwiched by a pair of electrodes and dried for gelatinization at room temperature for 12 h (separator is filter paper of  $\approx 1.2 \times 2.7 \text{ cm}^2$  of area and  $\approx 140 \mu\text{m}$  of thickness, electrodes are CC or 3-CC of  $\approx 1 \times 2.5 \text{ cm}^2$  for large-sized, or  $\approx 2 \times 20 \text{ cm}^2$  for large-sized). The 3 M tape and cling film were used as package materials and a Ni belt (thickness:  $\approx 100 \mu\text{m}$ ) as the lead. For the fiber supercapacitor, after partially immersing the same two fiber electrodes into gel electrolyte ( $\approx 3 \text{ cm}$  in length and  $\approx 500 \mu\text{m}$  in diameter) for several minutes, the electrodes are pulled out



and then put on the top of a piece of cling film in parallel with a space of  $\approx 1$  mm. They were then covered with the PVA/LiCl gel electrolyte and dried for gelatinization at room temperature for 12 h to fabricate a fiber supercapacitor as shown in Figure S10 in the Supporting Information.

**Characterizations:** The morphologies of CC, 3-CC were characterized by field-emission SEM (Hitachi S-4800) and TEM (FEI Tecnai F30, operated at 300 kV). Nitrogen adsorption/desorption was carried out at 77 K on ASAP 2027 specific surface area and pore diameter analyzer and sample was degassed at 200 °C for 6 h under vacuum prior to the measurement. The chemical component was analyzed on a multifunctional X-ray photoelectron spectroscope (PHI-5702, Mg K $\alpha$  X-ray, 1253.6 eV). Raman spectra measurement was recorded on a micro-Raman spectroscope (JY-HR800, 532-nm wavelength YAG laser).

**Electrochemical Measurements:** Electrochemical tests were carried out in 1 M of Na<sub>2</sub>SO<sub>4</sub> electrolyte at 25 °C. The electrochemical properties of CC and 3-CC (mass per unit area:  $\approx 21$  mg cm<sup>-2</sup>;  $\approx 19$  mg cm<sup>-2</sup>, area:  $\approx 1 \times 1.5$  cm<sup>2</sup>) were evaluated in a three electrode configuration (SCE as a reference electrode). Electrochemical impedance spectroscopy measurements were obtained at open circuit potential with the frequency ranging from 100 kHz to 10 mHz at an amplitude of 5 mV. The long-term cycle was evaluated by galvanostatic charge/discharge measurements. The capacitances were obtained from galvanostatic discharge curves according to the formulas:  $C_A = (I\Delta t)/(S\Delta V)$ ,  $C_V = C_A \times 20$ ,  $C_m = C_A/m$ , where  $I$  is the constant discharge current density,  $\Delta t$  the discharge time,  $S$  the area of device,  $\Delta V$  voltage drop upon discharging,  $m$  the mass density of electrode,  $C_A$  areal capacitance,  $C_V$  volume capacitance, and  $C_m$  mass capacitance. 1 mAh = 3.6 C. For fibered-shaped devices, the length capacitance ( $C_L$ ) from galvanostatic discharge curves was calculated according to the formula:  $C_L = (I\Delta t)/(L\Delta V)$ , where  $I$  is the constant discharge current density,  $\Delta t$  the discharge time,  $L$  the length of fiber electrode, and  $\Delta V$  voltage drop upon discharging. The areal capacitance ( $C_A$ ) was calculated according to  $C_A = C_L \times 10 \times 2$ ,  $C_V = C_A \times 20$ , and  $C_m = C_L/m$ , where  $C_L$  is the length mass density of two fiber electrodes. The energy densities were calculated using:  $E_L = C_L V^2/7200$ ,  $E_A = E_L \times 10 \times 2$ ,  $E_V = E_A \times 20$ ,  $E_m = C_m \times V^2/7.2$ . For planar devices, the capacitance was calculated using:  $C_A = (I\Delta t)/(S\Delta V)$ , where  $I$  is the constant discharge current density,  $\Delta t$  the discharge time,  $S$  the working area of device, and  $\Delta V$  voltage drop upon discharging. The energy densities were obtained according to  $E_A = C_A V^2/7200$ ,  $E_V = E_A \times 10$ , and  $E_m = C_A/m$ . And the power density was obtained according to  $P_x = E_x \times 3600/\Delta t$ , where  $x$  represents  $L$ ,  $A$ ,  $V$ , and  $m$ .<sup>[44]</sup>

## Supporting Information

Supporting Information is available from the Wiley Online Library or from the author.

## Acknowledgements

This work was supported by the National Natural Science Foundation of China (Grant No. 61376011). T.Q. made a greater contribution than the other authors.

## Conflict of Interest

The authors declare no conflict of interest.

## Keywords

all-solid-state symmetric supercapacitors, carbon fiber cloth, flexible and wearable, ultrahigh energy density

Received: February 15, 2017  
Revised: April 8, 2017  
Published online: July 14, 2017

- [1] Q. Huang, D. Wang, Z. Zheng, *Adv. Energy Mater.* **2016**, *6*, 1600783.
- [2] Y. Yang, Q. Huang, L. Niu, D. Wang, C. Yan, Y. She, Z. Zheng, *Adv. Mater.* **2017**, *29*, 1606679.
- [3] C. Liu, Z. G. Neale, G. Cao, *Mater. Today* **2016**, *19*, 109.
- [4] Q. Zhang, E. Uchaker, S. L. Candelaria, G. Cao, *Chem. Soc. Rev.* **2013**, *42*, 3127.
- [5] S. L. Candelaria, Y. Shao, W. Zhou, X. Li, J. Xiao, J.-G. Zhang, Y. Wang, J. Liu, J. Li, G. Cao, *Nano Energy* **2012**, *1*, 195.
- [6] L. Dong, C. Xu, Y. Li, Z.-H. Huang, F. Kang, Q.-H. Yang, X. Zhao, *J. Mater. Chem. A* **2016**, *4*, 4659.
- [7] L. Wen, F. Li, H. M. Cheng, *Adv. Mater.* **2016**, *28*, 4306.
- [8] X. Wang, X. Lu, B. Liu, D. Chen, Y. Tong, G. Shen, *Adv. Mater.* **2014**, *26*, 4763.
- [9] W. Wang, W. Liu, Y. Zeng, Y. Han, M. Yu, X. Lu, Y. Tong, *Adv. Mater.* **2015**, *27*, 3572.
- [10] K. Xu, W. Li, Q. Liu, B. Li, X. Liu, L. An, Z. Chen, R. Zou, J. Hu, *J. Mater. Chem. A* **2014**, *2*, 4795.
- [11] J. Yu, W. Lu, J. P. Smith, K. S. Booksh, L. Meng, Y. Huang, Q. Li, J.-H. Byun, Y. Oh, Y. Yan, T.-W. Chou, *Adv. Energy Mater.* **2016**, *6*, 1600976.
- [12] Y. Fu, X. Cai, H. Wu, Z. Lv, S. Hou, M. Peng, X. Yu, D. Zou, *Adv. Mater.* **2012**, *24*, 5713.
- [13] J. Bae, M. K. Song, Y. J. Park, J. M. Kim, M. Liu, Z. L. Wang, *Angew. Chem.* **2011**, *50*, 1683.
- [14] G. Qu, J. Cheng, X. Li, D. Yuan, P. Chen, X. Chen, B. Wang, H. Peng, *Adv. Mater.* **2016**, *28*, 3646.
- [15] J. Ren, L. Li, C. Chen, X. Chen, Z. Cai, L. Qiu, Y. Wang, X. Zhu, H. Peng, *Adv. Mater.* **2013**, *25*, 1155.
- [16] L. Liu, Y. Yu, C. Yan, K. Li, Z. Zheng, *Nat. Commun.* **2015**, *6*, 7260.
- [17] L. Dong, C. Xu, Y. Li, C. Wu, B. Jiang, Q. Yang, E. Zhou, F. Kang, Q. H. Yang, *Adv. Mater.* **2016**, *28*, 1675.
- [18] Y. Meng, Y. Zhao, C. Hu, H. Cheng, Y. Hu, Z. Zhang, G. Shi, L. Qu, *Adv. Mater.* **2013**, *25*, 2326.
- [19] X. Li, T. Zhao, Q. Chen, P. Li, K. Wang, M. Zhong, J. Wei, D. Wu, B. Wei, H. Zhu, *Phys. Chem. Chem. Phys.* **2013**, *15*, 17752.
- [20] H. Cheng, Z. Dong, C. Hu, Y. Zhao, Y. Hu, L. Qu, N. Chen, L. Dai, *Nanoscale* **2013**, *5*, 3428.
- [21] J. Ren, W. Bai, G. Guan, Y. Zhang, H. Peng, *Adv. Mater.* **2013**, *25*, 5965.
- [22] Y. Lv, F. Zhang, Y. Dou, Y. Zhai, J. Wang, H. Liu, Y. Xia, B. Tu, D. Zhao, *J. Mater. Chem.* **2012**, *22*, 93.
- [23] W. Xing, C. C. Huang, S. P. Zhuo, X. Yuan, G. Q. Wang, D. Hulicova-Jurcakova, Z. F. Yan, G. Q. Lu, *Carbon* **2009**, *47*, 1715.
- [24] Y. S. Yun, C. Im, H. H. Park, I. Hwang, Y. Tak, H.-J. Jin, *J. Power Sources* **2013**, *234*, 285.
- [25] C. Ma, Y. Song, J. Shi, D. Zhang, X. Zhai, M. Zhong, Q. Guo, L. Liu, *Carbon* **2013**, *51*, 290.
- [26] Y. Wen, T. Qin, Z. Wang, X. Jiang, S. Peng, J. Zhang, J. Hou, F. Huang, D. He, G. Cao, *J. Alloys Compd.* **2016**; <https://doi.org/10.1016/j.jallcom.2016.12.330>.
- [27] F. Bonaccorso, L. Colombo, G. Yu, M. Stoller, V. Tozzini, A. C. Ferrari, R. S. Ruoff, V. Pellegrini, *Science* **2015**, *347*, 1246501.
- [28] H. Jiang, P. S. Lee, C. Li, *Energy Environ. Sci.* **2013**, *6*, 41.
- [29] L. Wan, J. Wang, L. Xie, Y. Sun, K. Li, *ACS Appl. Mater. Interfaces* **2014**, *6*, 15583.
- [30] J. Wu, D. Zhang, Y. Wang, B. Hou, *J. Power Sources* **2013**, *227*, 185.
- [31] D. Hulicova-Jurcakova, M. Kodama, S. Shiraiishi, H. Hatori, Z. H. Zhu, G. Q. Lu, *Adv. Funct. Mater.* **2009**, *19*, 1800.
- [32] Y. Li, C. Lu, S. Zhang, F.-Y. Su, W. Shen, P. Zhou, C. Ma, *J. Mater. Chem. A* **2015**, *3*, 14817.
- [33] G. Xiong, C. Meng, R. G. Reifenberger, P. P. Irazoqui, T. S. Fisher, *Energy Technol.* **2014**, *2*, 897.
- [34] G. Wang, H. Wang, X. Lu, Y. Ling, M. Yu, T. Zhai, Y. Tong, Y. Li, *Adv. Mater.* **2014**, *26*, 2676.

- [35] S. J. Gregg, K. S. W. Sing, *Adsorption, Surface Area, and Porosity*, Academic Press, London **1982**.
- [36] H.-P. Cong, X.-C. Ren, P. Wang, S.-H. Yu, *Energy Environ. Sci.* **2013**, *6*, 1185.
- [37] J. Yan, Z. Fan, T. Wei, W. Qian, M. Zhang, F. Wei, *Carbon* **2010**, *48*, 3825.
- [38] T. Qin, B. Liu, Y. Wen, Z. Wang, X. Jiang, Z. Wan, S. Peng, G. Cao, D. He, *J. Mater. Chem. A* **2016**, *4*, 9196.
- [39] D. Ye, Y. Yu, J. Tang, L. Liu, Y. Wu, *Nanoscale* **2016**, *8*, 10406.
- [40] P. Suktha, P. Chiochan, P. Iamprasertkun, J. Wutthiprom, N. Phattharasupakun, M. Suksomboon, T. Kaewsongpol, P. Sirisinudomkit, T. Pettong, M. Sawangphruk, *Electrochim. Acta* **2015**, *176*, 504.
- [41] G. Wang, L. Zhang, J. Zhang, *Chem. Soc. Rev.* **2012**, *41*, 797.
- [42] Z. Fan, J. Yan, T. Wei, L. Zhi, G. Ning, T. Li, F. Wei, *Adv. Funct. Mater.* **2011**, *21*, 2366.
- [43] J. S. Wei, H. Ding, Y. G. Wang, H. M. Xiong, *ACS Appl. Mater. Interfaces* **2015**, *7*, 5811.
- [44] K. Jost, D. Stenger, C. R. Perez, J. K. McDonough, K. Lian, Y. Gogotsi, G. Dion, *Energy Environ. Sci.* **2013**, *6*, 2698.